1
Synthesis, Functionalization, and Characterization

Jianxun Xu, Xing Lu, and Baowen Li

1.1
Introduction

Recent years have witnessed tremendous development in the studies of carbon nanomaterials, including fullerenes, carbon nanotubes (CNTs), and graphene. These carbon nanomaterials solely comprise sp^2 carbon atoms, which form conjugated six-membered rings fused together with various numbers of five-membered rings. These novel materials, which exhibit unique structures and properties, are expected to be useful in many fields.

To achieve the proposed applications, it is of primary importance to synthesize these nanomaterials with defined structures in reasonable production yield. At the same time, it is always required to further modify their surface properties to optimize the interface environment where they function. The fine structure and the surface properties are critical for their biological effects. And, it is actually important to identify the comprehensive structure parameters and surface modifications for their toxicological evaluations and understanding the related mechanisms. In this chapter, we present the basic concept and the latest achievements in the synthesis of carbon nanomaterials and their functionalization, especially related to biological purposes. The state-of-the-art characterization methods are also critically reviewed.

1.2
Fullerenes and Metallofullerenes

There have been a tremendous amount literature describing the synthesis, characterization, structures, and properties of empty fullerenes. As a result, we will only focus on the achievements in the recent studies of endohedral metallofullerenes (EMFs), which are hybrid molecules formed by the encapsulation of metallic species into the fullerene cages in the following contexts.

Biomedical Applications and Toxicology of Carbon Nanomaterials, First Edition.
Edited by Chunying Chen and Haifang Wang.

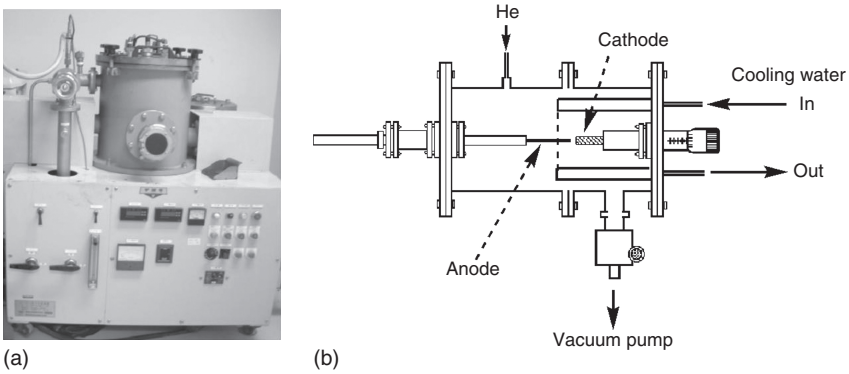

Figure 1.1 (a) An arc discharge reactor used to synthesize EMFs and (b) its schematic illustration.

1.2.1
Synthesis and Purification

1.2.1.1
Synthesis

The synthesis of empty fullerenes can be achieved rather easily via such methods as initial laser ablation, then arc discharge, and finally combustion of aromatic organic molecules even under ambient conditions. However, to produce EMFs, harsher conditions are always required to evaporate the metals into the gas phase. As such, only laser ablation and arc discharge approaches are effective.

Smalley and colleagues made the first attempt by using laser ablation equipment. A composite graphite disk doped with lanthanum oxide was irradiated with laser in a quartz tube under an inert atmosphere. The tube was heated to a temperature higher than 800 °C in order to ensure the formation of fullerenes and EMFs [1–3].

This is the most powerful and convenient method for EMF production (Figure 1.1). By allowing N_2 or NH_3 into the chamber, or by adding some nitrogen-containing compounds into the graphite rod, metal nitride cluster EMFs are readily obtained [4, 5]. EMFs containing a metal oxide cluster (Sc_4O_3) [6], a metal sulfide cluster (Sc_2S) [7], or even a metal cyanide cluster (Sc_3NC) have been synthesized by introducing the corresponding heterogeneous additives into the reactor.

1.2.1.2
Purification

Extraction Solvent extraction is the most common method and frequently used in the first step of fullerenes separation from soot. Generally, 1,2,4-trichlorobenzene (TCB) shows the highest affinity toward the fullerene species. Alternatively,

1,2-dichlorobenzene (ODCB), chlorobenzene, toluene (xylene, benzene), and CS_2 are also commonly used to extract fullerenes and EMFs [8–10].

On the other hand, electrochemical methods were also used for the extraction of insoluble EMFs. The insoluble species can be made soluble by altering the electronic properties of these insoluble species. Diener and Alford made the first attempt, and obtained a mixture of insoluble, small-bandgap fullerenes such as C_{74}, Gd@C_{60}, and Gd@C_{74} by electrochemical reduction of the sublimate of Gd-containing soot [11]. In addition, some insoluble EMFs were extracted after increasing the solubility via chemical derivatization. For example, upon extraction with 1,2,4-trichlorobenzene of La-containing soot, some insoluble species such as La@C_{2n} ($2n = 72–82$) were functionalized by the trace dichlorophenyl radicals generated during refluxing [12–16].

HPLC Separation Complete separation of EMFs has been accomplished only by high-performance liquid chromatography (HPLC) [17–19], which has proven to be the most powerful and frequently used technique for the separation of EMFs. The HPLC technique utilizing different modified HPLC columns can even afford the separation of structural cage isomers of various EMFs. Five complementary HPLC columns are available commercially: PYE, PBB, NEP, Buckyprep, and Buckyprep M.

Non-HPLC separation Electrochemical studies of EMFs have indicated that their redox potentials are quite different from those of empty fullerenes, so electrochemical methods can be efficiently used for separating EMFs from the latter. In 2003, Bolskar and Alford designed a separation protocol based on the electrochemical as well as chemical oxidation of EMF extracts by $AgPF_6$, $AgSbCl_6$, and tris(4-bromo-phenyl)aminium hexachloroantimonate [20].

Moreover, the "SAFA" (stir and filter approach) was proposed by Stevenson *et al.* [21, 22]. Without using any chromatography equipment, the authors used cyclopentadienyl and amino-functionalized silica to selectively bind contaminant fullerenes (empty fullerenes and non-nitride clusterfullerenes) and claimed to obtain the purified nitride clusterfullerenes under optimum conditions [21]. This method could also be used to separate $Sc_3N@C_{80}$-I_h and $Sc_3N@C_{80}$-D_{5h} isomers [22].

1.2.2 Chemical Functionalization

1.2.2.1 Carbene Reaction

Carbene reaction is used frequently to functionalize many different kinds of EMFs; this is mainly due to its highly selectivity. For example, through photoirradiation or even heating, reactions of M@C_{2v}-C_{82} (M = La, Y, Pr, Gd, etc.) with 2-adamantane-2,3-[3*H*]-diazirine (AdN_2) were conducted and two monoadducts of M@C_{2v}-C_{82} were obtained [23]. The single-crystal results

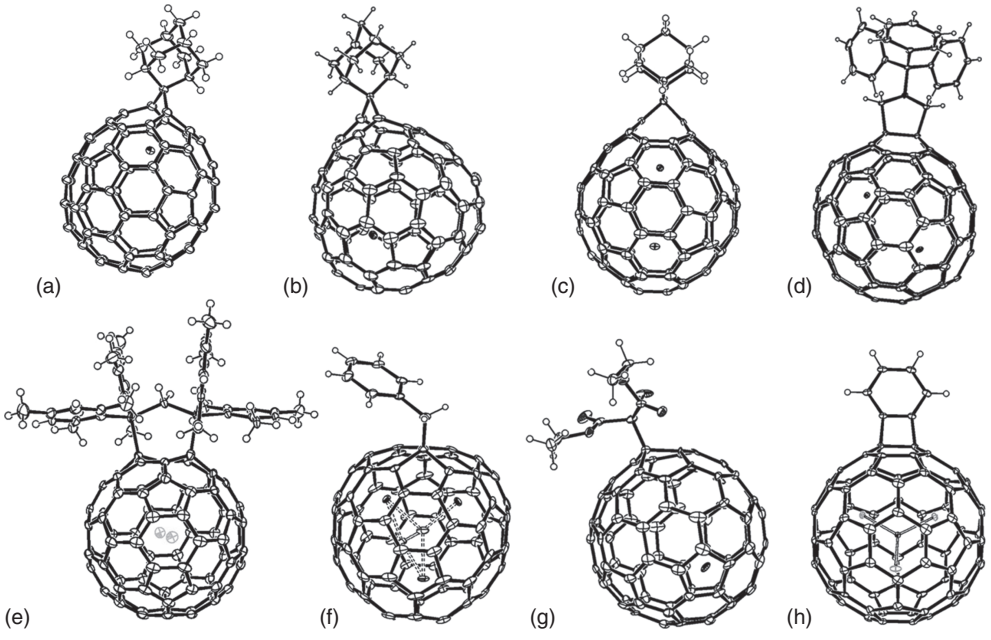

Figure 1.2 Ortep drawings of (a) $Y@C_{82}-Ad$, (b) $Yb@C_{84}Ad$, (c) $La_2@C_{80}-Ad$, (d) $La_2@C_{80}-NTrt$, (e) $Ce_2@I_h-C_{80}-(Mes_2Si)_2CH_2$, (f) $Sc_3C_2@C_{80}-CH_2C_6H_5$, (g) $La@C_{82}-CBr(COOC_2H_5)_2$, (h) $Sc_3N@C_{80}-C_6H_4$.

(Figure 1.2a) revealed that the addition always took place on those carbon atoms near the metal atom. Similar reaction of dimetallofullerenes $M_2@C_{80}$ (M = La, Ce) were carried out by Akasaka's group. The single-crystal X-ray structure (Figure 1.2c) analysis of monoadduct $La_2@C_{80}Ad$ confirmed that two La atoms were interestingly collinear with the spiro carbon of the Ad group and the distance between La atoms is increased [24]. Recently, the carbene reaction has been used to investigate the chemical properties of divalent EMFs. Reaction of $Yb@C_{80}$ with AdN_2 reported by Lu in 2013 resulted in the first derivative of a divalent metallofullerene. Only one isomer was obtained, indicating the high regioselectivity of this reaction [25]. $Yb@C_{84}$ (Figure 1.2b) was used to react with AdN_2 in the same year. Theoretical calculations suggest that the addition of divalent EMFs is mainly driven by the release of the local strains of cage carbons rather than by charge recombination, which is always prominent due to the affinity of typical trivalent EMFs [26].

1.2.2.2 Bingel–Hirsch Reaction

The Bingel–Hirsch reaction is one of the famous nuclophilic reactions in fullerene chemistry. The reactions of diethyl bromomalonate with metallofullerenes in the presence of 1,8-diazabicyclo[5.4.0]-undec-7ene (DBU) are extremely aggressive, so it is always used to synthesize various adducts. Surprisingly, Akasaka obtained

a singly bonded monoadduct of La@C_{82}(La@C_{82}CBr($COOC_2H_5$)$_2$) (Figure 1.2g) by means of the Bingel–Hirsch reaction [27].

1.2.2.3

Prato Reaction

Many investigations of Prato reaction of metallofullerenes indicate that changing the substituted group of aldehydes is a very efficient approach to obtain metallofulleropyrrolidines with different branched chains. This method is widely used to introduce functional groups for further photophysical studies. The first Prato reaction of EMFs was carried out by adding azomethine ylide into La@C_{82} solution. Two major endohedral metallofulleropyrrolidines, a monoadduct and a bisadduct of La@C_{82}, were isolated with HPLC, which suggested that the reaction is regioselective to some extent. A special Prato reaction of M_2@C_{80} (M = La, Ce) with 3-triphenylmethyl-5-oxazolidinone (NTrt) was reported by Akasaka's group; the [6,6]- and [5,6]-adducts resulted were and characterized. The X-ray crystallographic analysis of the [6,6]-adduct (Figure 1.2d) confirmed that the metal atoms are fixed, which is opposite of the random circulation in pristine La_2@C_{80} [28].

1.2.2.4

Bis-Silylation

Bis-silylation of La@C_{2v}–C_{82} reported by Akasaka *et al.* in 1995 was the first exohedral chemical functionalization of metallofullerenes [29]. Afterward, they succeeded likewise in the bis-silylation of M@C_{2v}–C_{82} (M = Gd, Y, Ce) and M@C_s-C_{82} with disilirane through a photochemical or thermal pathway [30]. Similar works of di-EMFs such as M_2@C_{80} (M = La, Ce) (Figure 1.2e) were conducted by Akasaka. In 2006, the reaction of trimetallic nitride-templated endohedral metallofullerene (TNT EMF) Sc_3N@C_{80} with 1,1,2,2-tetramesityl-1,2-disilirane under photoirradiation was carried out. Both 1,2- and 1,4-cycloadducts were successfully isolated and completely characterized by NMR measurement and single-crystal X-ray structure analysis.

1.2.2.5

Diels–Alder Reaction and Benzyne Reaction

Cyclopentadiene (Cp) and 1,2,3,4,5-pentamethylcyclopentadiene (Cp*) were used to participate in the [4 + 2] reaction of La@C_{82}. Interestingly, Diels–Alder reactions of La@C_{82} with Cp was reversible even at 298 K, which was proved through HPLC. X-ray analysis of La@C_{82}Cp* showed that 60% of the monoadduct formed a dimer in the solid state [31]. Benzyne reaction of La@C_{82} was undertaken by Lu in 2010, and the X-ray crystallographic structure analysis of the adduct showed that two benzyne moieties were attached to the highly pyramidized section and NO_2 was unexpectedly linked to cage [32]. Later on, two similar benzyne reactions of Sc_3N@C_{80} (Figure 1.2h) were reported by Echegoyen and Wang in 2011. Besides the typical cycloadditions above, some uncommon cycloadditions

of metallofullerenes such as radical malonate addition, azide addition, zwitterion addition, carbosilylation, so on, were investigated as well to some extent [30].

1.2.2.6 Singly Bonded Addition

The thermal reaction of La@C_{82} with 3-triphenylmethyl-5-oxazolidinone (NTrt) reported by Akasaka in toluene afforded the benzyl monoadducts La@C_{82}($CH_2C_6H_5$), Surprisingly, the same monoadducts were also obtained by the photoirradiation of La@C_{2v}–C_{82} in toluene without NTrt [33]. In 2008, Dorn obtained a dibenzyl adduct M_3N@C_{80}($CH_2C_6H_5$)$_2$ (M = Sc, Lu) by photochemical reactions of M_3N@C_{80} (M = Sc, Lu) with benzyl bromide, and confirmed the structure of 1,4-dibenzyl adduct of M_3N@C_{80} (M = Sc, Lu) by X-ray crystallographic analysis [34]. Recently, photochemical reaction of Sc_3C_2@C_{80} with benzyl bromide was undertaken by Lu, in 2014. X-ray structure analysis (Figure 1.2f) demonstrated that the cluster configuration in EMFs was highly sensitive to the electronic structure, which is tunable by exohedral modification [35]. Another typical singly bonded addition of EMFs is perfluoroalkylation. Perfluoroalkylation of metallofullerens, which is a special solid–solid reaction, prefers to afford various multiadducts. CH_3I and Ag(CF_3CO_2) are widely used as reagents for the perfluoroalkylations of EMFs. Reactions of Sc_3N@C_{80} were the most investigated because of the less selectivity of perfluoroalkylation and relatively large amount of Sc_3N@C_{80}. After persistent efforts, single crystals of the multiadduct Sc_3N@C_{80}(CF_3)$_n$ (n = 14, 16) were obtained by Yang and coworkers [30]

1.2.2.7 Supramolecular Complexes of EMFs

Supramolecular complexes based on metallofullerenes with macrocycles or organic donors have been investigated because of its attractive electron transfer behavior. In 2006, Akasaka and colleagues synthesized complexes of La@C_{82} with 1, 4, 7, 10, 13, 16-hexaazacyclooctadecane. The complexes, which precipitate in toluene, are soluble in polar solvents. According to this phenomenon, they successfully separated metallofullerenes from soot extracts selectively [36]. Another organic donor, *N*,*N*,*N*′*N*′-tetramethyl-*p*-phenylenediamine (TMPD), was also used to form complexes with La@C_{82}; the characterization with spectroscopy and ESR confirmed the reversible intermolecular electron transfer system at complete equilibrium in solution and the formation of stable diamagnetic/paramagnetic anions of La@C_{82} and radical anions of the donor, respectively [37].

1.2.3 Characterization

1.2.3.1 Synchrotron Radiation Powder Diffraction (SRPD)/Rietveld/MEM

This method is the earliest to confirm EMFs [38]. In 1995, Takata *et al.* reported the MEM maps of Y@C_{82} and C_{82} and confirmed that the metal atom is indeed

encapsulated inside the fullerene cage [38]. Thereafter, the structures of numerous EMFs were determined similarly, such as those of Sc@C_{82}, La@C_{82}, and Y_2C_2@C_{82} [39–41]. This experiential strategy is not always reliable because several erroneous structures have been assigned using this method [42, 43].

1.2.3.2

Nuclear Magnetic Resonance (NMR) Spectroscopy

NMR spectroscopy was also used to characterize structures. The cage structures of many trivalent EMFs have been established, especially those of M@C_{82}, showing that both C_{2v}(9)-C_{82} and C_s(6)-C_{82} cages are favorable, with the former being much more stable. Furthermore, using the two-dimensional incredible natural abundance double quantum transfer experiment (INADEQUATE), bond connectivities among nonequivalent cage carbons were also modeled in cases where the NMR spectrum was sufficiently clear [44, 45]. Recently, the signals from the internal C_2 unit of carbide cluster EMFs were detected with NMR spectrometry using ^{13}C-enriched samples. For the Sc_2C_2 cluster, which is frequently encountered in carbide cluster EMFs, peaks of the C_2 unit are observed between 220 and 260 ppm, but the corresponding signal of the C_2 motif in the Sc_3C_2@I_h(7)-C_{80} anion was shifted downfield to 328 ppm [46–49]. For divalent EMFs, di-EMFs, and cluster EMFs, which are all diamagnetic species, direct NMR measurements are valid for establishing their structures [50–52].

1.2.3.3

Theoretical Calculation

Calculations can predict the relative stabilities of EMF by considering the charge transfer from the encapsulated metals to the carbon cage [48, 53]. A "maximum pentagon separation rule" proposed by Poblet and coworkers stated that the pentagonal carbon rings on the fullerene cage tend to accumulate negative charges transferred from the internal metallic species. Consequently, they are separated to the greatest degree over the cage, engendering the maximum separation of the positively charged internal metal cations.

1.2.3.4

Single-Crystal X-ray Diffraction Crystallography

It is the most reliable solution to molecular structures. The EMF can form neat co-crystals with metal porphyrins: M^{II}(OEP) (M = Ni, Co etc., OEP = 2,3,7,8,12,13,17,18-octaethylporphyrin dianion) as the eight alkyl groups of M^{II}(OEP) wrap the spherical molecule. Balch and colleagues have also obtained the structure of Kr@C_{60}, indicating that the inert gas molecule is at the center of the cage [54]. In contrast, the single metal in mono-EMFs always departs from the center of the cage, either approaching closely to a hexagonal carbon ring for rare-earth metals or over a carbon bond for alkali metals, for example, M@C_{3v}(134)-C_{94}(M = Tm, Ca) [55]. In large cages, it is also possible for the single metal to move even at low temperatures (e.g., Sm@C_{90} isomers) [56]. It is noteworthy that the crystal of Li^+@C_{60} was obtained by co-crystallization with

its counter anion, $[SbCl_6]^-$, instead of metal porphyrin [57]. Furthermore, it was found in a recent study that the solvated $Sc_3N@C_{80}$ are nicely ordered in the crystal lattice, providing new insight into the structures of "pristine" EMFs [58].

1.2.3.5 Others

In addition to the methods that can be viewed as direct solutions to the molecular structure of EMFs, means such as infrared spectroscopy, Raman spectroscopy, absorption spectroscopy, electrochemical spectroscopy, and even high-resolution tunneling electronic microscopy (HRTEM) have all been used to characterize EMFs.

1.2.4 Questions and Future Directions

The development and structural recognition of fullerenes and metallofullerenes have a long way to go. The availability of EMFs is much less than sufficient for scientific research or practical application. Except for $Sc_3N@C_{80}$, other EMF species yielded less using the arc discharge method, and are more difficult to separate, because of the numerous structural isomers and low stability. As a result, more powerful synthetic methods and more efficient separation process are urgently needed to increase the availability of EMFs.

Practical applications of these fascinating materials also demand detailed exploration. Because of the presence of the metallic species, which are the mainstay of many novel electronic, magnetic, and optic applications, every detail of the functions of both the fullerene cage and the metallic core must be investigated.

1.3 Carbon Nanotubes

CNTs, including single-walled carbon nanotubes (SWCNTs) and multi-walled carbon nanotubes (MWCNTs), can be imagined as cylinders by rolling up hexagonal carbon sheets. The diameter and the chirality of a SWCNT can be defined in terms of its chiral vector (*m, n*), which determines the direction of rolling the carbon sheet, as illustrated in Figure 1.3. It is fantastic that SWCNTs with different (*m*, *n*) values exhibit different electrical (metallic or semiconducting) and optical properties in spite of the same chemical composition and bonding behaviors [59].

CNTs were probably observed for the first time using transmission electron microscopy (TEM) in the 1970s. But, only after Iijima *et al.*'s reports on their discovery and structural characterizations on MWCNTs in 1991 and SWCNTs in 1993, researchers around the world started to intensively study this kind of new materials, which have been proven to possess outstanding mechanical, thermal, optical, and electrical properties [59–61]. Various potential applications of CNTs

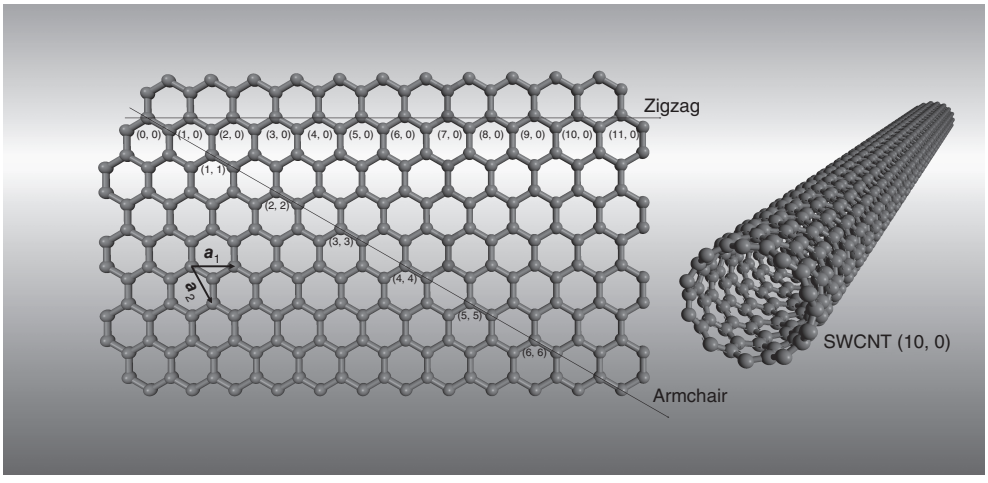

Figure 1.3 A carbon nanotube can be regarded as a cylinder obtained by rolling up a graphene sheet. The vector convention is used to define the points in the graphene lattice. The illustrated SWCNT (10, 0) is formed by superimposing the point (10, 0) with (0, 0) in the graphene sheet, which is a zigzag tube.

are expected for composites, flat panel displays, electronic nano-devices, sensors, functional probes, drug delivery systems, and so forth [62–67].

1.3.1 Synthesis

The widely used methods to synthesize CNTs are arc discharge, laser ablation, and chemical vapor deposition (CVD).

1.3.1.1 Arc Discharge Method

An arc discharge can be used to produce various carbon nanomaterials, including fullerenes, CNTs, and carbon nanohorns. It is an effective way to synthesize high-quality CNTs having different structural features. The SWCNTs and MWCNTs observed by Iijima in his pathbreaking work were actually obtained by means of arc discharge. The facility is very similar to that used to produce fullerenes described previously (Figure 1.1). Under optimal conditions of arcing between two high-purity graphite electrodes, MWCNTs can be synthesized. SWCNTs can be generated by arc discharge only when suitable metal catalysts are used, including Fe, Co, Ni, Pt, and Rh [61, 68, 69]. CNTs produced by arc discharge have few structural defects, which helps in preserving the unique properties of CNTs. Meanwhile, it also causes problems to handle these CNTs in wet processes. For example, it is difficult to disperse such CNT powders well in the aqueous phase when researchers aim to use CNTs for biological applications.

1.3.1.2

Laser Ablation Method

Laser ablation is another method developed for CNT synthesis at the early stage of studies on carbon nanomaterials. Carbon evaporated from high-purity graphite source under high-power YAG laser irradiation can form MWCNTs at 1200 °C in an Ar or a N_2 atmosphere [70]. When metal catalysts (Co–Ni) were mixed into the graphite target, SWCNT bundles were synthesized [71]. On the other hand, spherical aggregates of single-walled carbon nanohorns were obtained in the absence of any catalyst at room temperature [72, 73]. Currently, laser ablation method is not widely adopted for CNT synthesis because of the necessity of high-power lasers and high-purity graphite.

1.3.1.3

CVD Method

Many research groups and commercial manufacturers are using CVD for the synthesis of CNTs, which is a versatile and economic method to produce different types of CNTs and graphene (discussed below). In the CVD process, carbon sources in the gas phase flowing through a heating furnace decompose and dissolve on the surface of active catalyst nanoparticles, initiating the growth of CNTs. Since the successful CVD growth of SWCNTs in the late 1990s, a huge amount of work has been reported on growing CNTs by this technique [74–78]. It has been revealed that various CNTs with different morphologies and crystallinity can be generated by adjusting the parameters including the carbon feedstock, catalyst (composition, size, shape, density, and crystal structure), carrier gas, temperature, and even the direction of gas flow and tube furnace. Furthermore, aligned CNTs (vertical or horizontal) with designed patterns can also be obtained based on the CVD technique [79–81].

1.3.1.4

Synthesis of CNTs with a Defined Structure

Nowadays, it has been realized that the crucial point for practical applications of CNTs is to obtain sufficient amount of a single type of CNTs with defined diameter and chirality. Many research groups have contributed to this effort by optimizing the characteristics of the catalysts used in the CVD process. For example, Harutyunyan *et al.* increased the fraction of metallic SWCNTs up to 91% by optimizing the thermal annealing conditions of the Fe nanocatalyst [82]. Wang *et al.* reported their work on the growth a single type of SWCNTs (9, 8) with 51.7% abundance by using a sulfate-promoted $CoSO_4/SiO_2$ catalyst [83]. Most recently, Li and colleagues successfully obtained specific SWCNTs (12, 6) with an abundance over 92% in their CVD growth studies [84]. W_6Co_7 alloy nanoclusters with specific structural features were used as the catalyst and believed to be the key factor to initialize the SWCNT's specific growth. These works demonstrated the possibility to directly grow structure-controlled CNTs, which is of great importance to achieve CNT applications for nanoelectronics and biological purposes.

1.3.2 Functionalization

Before applying CNTs to a certain applications, it is usually required to modify the surface of CNTs for functionalization, better dispersion, and feasible manipulation. There have been a large number of reports on the surface modifications of CNTs, which can be generally classified as covalent chemistry and noncovalent modifications.

1.3.2.1 Covalent Chemical Reactions

There are usually some impurities (amorphous carbon, catalyst particles, etc.) in the raw soot of CNTs. During the purification processes using acid oxidation, oxygenated functional groups are induced onto CNTs, mainly carbonyl and carboxylic groups. The most widely used covalent chemical reactions of CNTs are through amidation based on the carboxylic groups on the surface or the open ends of the nanotubes. Many other chemical reactions, such as Prato reaction, halogenation, cycloaddition, necleophilic addition, and radical addition, among others, have also been reported. The related reaction route, mechanism, and characterizations have been reported in several reviews [85, 86].

1.3.2.2 Noncovalent Modifications

Wrapping the CNTs with surfactants, biomolecules, and various types of polymers is another effective way to disperse and functionalize CNTs. This approach takes advantage of the nonspecific interactions (mainly hydrophobic affinity and $\pi-\pi$ stacking) between the graphite surface of CNTs and hydrophobic moieties or aromatic rings of the reactants. A wide variety of surfactants (ionic and nonionic) have been used to wrap and disperse CNTs, such as sodium dodecyl sulfate, sodium cholate, sodium pyrenebutyrate, Tween, Triton, and so on. It has been found that bile salts are exceptionally effective for dispersing CNTs due to their unique structure comprising a steroid ring and facial amphiphiles [87, 88]. These types of surfactants were utilized to obtain stable, monodispersed SWCNTs suitable for diameter sorting using density gradient ultracentrifugation.

Modification Using Biomolecules Different types of biomolecules are used for the dispersion and functionalization of CNTs. Among them, DNA molecules have proven to be highly effective through helical wrapping onto the CNT surface [89]. On the basis of their outstanding dispersion efficiency, DNA sequences were able to further recognize and separate structure-specific CNTs [90]. Moreover, phosphate lipid-functionalized short CNTs can self-insert into lipid bilayers and live cell membranes to form biomimetic ion channels able to transport water, protons, small ions, and DNA [91]. Some proteins, such as bovine serum albumin and streptavidin, were also widely used for surface modification and possible further functionalization of CNTs, especially for biological applications.

Modification Using PEG-based Polymers The integration between CNTs and polymers has been extensively investigated. To fabricate high-performance CNT–polymer composites, CNTs were dispersed and bonded with various species of polymers, such as poly(acrylate), hydrocarbon polymers, and conjugated polymers, to name a few [85]. Meanwhile, for biological purposes, block copolymers comprising hydrophobic chains and hydrophilic poly(ethylene glycol) (PEG) are the most widely used reagents to modify and disperse CNTs in highly salted aqueous solutions and biofluids [92]. It is well known that the PEG moieties over the CNT surface can prevent nonspecific protein adsorption and increase the biocompatibility of CNTs. PEG chains with different lengths and branch structures have been attached to CNTs. Among them, phosphate–lipid conjugated PEG polymers were the most commonly used to form stable suspension of CNTs in solutions with high ionic strength [93]. A comb-shaped PEG branch was proven to have higher dispersion efficiency as a result of the higher density of PEG chains above the hydrophobic graphite surface [94]. It was also possible to further enhance the dispersion ability of PEG polymers by adjusting the linker structure between the hydrophobic and the PEG chains. For example, it was found that ceramide-conjugated PEG, which has a neutral linker group, possesses a higher dispersion potential than the corresponding charged phospholipid-conjugated PEG polymers [95].

1.3.3
Characterization

Different from real molecules, a CNT sample is actually a mixture containing CNTs with different diameters, lengths, and chirality. They cannot form real solutions or identical crystals. Therefore, many analysis methods commonly used in molecular chemistry, such as X-ray diffraction crystallography, NMR, and so on, are not effective for identifying the exact chemical composition and binding information of CNTs and the attached functional groups. Alternative methods are adopted to obtain the structural features of CNTs and functionalized derivatives to some extent, which include transmission electron microscopy (TEM), atomic force microscopy (AFM), Raman spectroscopy, ultraviolet–visible (UV–vis) absorbance spectroscopy, and near-infrared (NIR) fluorescence.

1.3.3.1
Microscopic Characterizations

Among these analysis tools, TEM is a widely used method to characterize CNTs with respect to their morphology and composition information. It is also a powerful tool to study *in situ* dynamic processes in the nanoscale. For example, Suenaga *et al.* [96] were able to directly image Stone–Wales defects in SWCNTs and their propagation under heating by means of high-resolution TEM with atomic resolution. The development of this technique in recent years has made it possible to achieve elemental analysis using electron energy loss spectroscopy to an

unprecedented sensitivity, even at the atomic level [97]. Compared to TEM, AFM is more versatile and nondestructive. The morphology and conformation of the attached soft materials on the surface of CNTs, such as DNA and proteins, were able to be analyzed by AFM observations [98]. Moreover, tip-enhanced Raman spectroscopy integrated with AFM is regarded as a fantastic tool for chemical analysis at the nano-scale [99]. It holds promise to detect single molecules on surfaces, although the current sensitivity is still limited by the use of conventional AFM tips. The newly developed multiple-probe AFM is a specialized method that allows researchers to manipulate up to four AFM probes at the same time [100]. It affords flexible and precise control of the tip location and tip–sample force when the tips are used as electrodes for probing the electrical properties of individual CNTs.

1.3.3.2 Spectroscopic Characterizations

Spectroscopic methods are also very useful in obtaining structural information of CNTs, which is especially important to identify the functionalized chemical species on CNTs. Raman spectroscopy is a versatile and sensitive tool that has been utilized from the very beginning of CNT studies [101, 102]. It is possible to identify a single CNT based on its resonance Raman spectrum, giving structural characteristics including the diameter, defect density, surface functionality, and much beyond. It has been a standard tool in the studies of nanocarbon materials. UV–vis absorbance and NIR fluorescence are commonly used to analyze CNT samples dispersed in solution [103]. Both methods are very sensitive to the dispersion state of functionalized CNTs in solution (individuals or bundles). Especially, UV–vis measurements are very easy to perform, and can give valuable information of CNTs on the dispersion state, preliminary chemical functional components, diameter, chirality, and even the length.

1.3.4 Questions and Future Directions

Based on their outstanding structural features and properties, CNTs are expected to be used in various applications, including electronic devices, sensors, and biological uses. However, to effect these practical applications, it is necessary to obtain the CNT samples having a defined structure. The diameter, chirality, and even the length of a CNT affect its electrical and biological properties. As mentioned above, researchers have been able to synthesize CNT samples with identical chirality. It is also possible to separate CNTs having a certain structural feature by density-gradient ultracentrifugation. But, until now, the amount of the pure CNTs produced is too small to be applied to practical applications. It is of critical importance to produce pure CNTs of a defined structure in a reproducible and economical way to achieve practical applications of this amazing material after over two decades of its discovery.

1.4 Graphene

Graphene, a single sp^2-bonding carbon layer of the graphite structure, is a basic building block for graphitic materials of all other dimensionalities. It can be wrapped up into 0D fullerenes, rolled into 1D nanotubes, and stacked into 3D graphite (Figure 1.4a) [104]. It has potential to exhibit a wide range of remarkable structural and transport properties, for example, specific surface area, high carrier mobility (>200 000 $cm^2 V^{-1} s^{-1}$) [108, 109], high Young's modulus (~1100 GPa) [110], excellent optical transparency [111], and high thermal conductivity (~5000 $W m^{-1} K^{-1}$) [112]. These peculiar properties arise from its unique electronic band structure, in which the conduction band overlaps with the valence band at two points (K and K′) in the Brillouin zone, and in the vicinity of these points the electron energy exhibits a linear relationship with the wave vector (Figure 1.4b) [105]. The experimental observations of the extraordinary transport properties have fueled extensive research on its chemical and physical properties [113, 114]. Although the experimentally observed values are substantially lower than theoretical predictions, research into graphene to date has highlighted the potential for applications in nanodevices, energy-storage materials, polymer composites, liquid crystal devices, and biomedicine [115, 116]. In this section, we aim to summarize the progress made on graphene, ranging from the synthesis and characterization to functionalization. Clearly, the development of various methods for producing graphene with controllable quality, quantity, and morphology might enable us to expand the graphene family with fascinating properties.

1.4.1 Synthesis and Characterization

In extensive studies to date, four different routes have been reported to produce graphene. The first was the micromechanical exfoliation of graphite, named as the "Scotch tape" or peel-off method [113]. This approach was inspired by earlier work on the micromechanical exfoliation from patterned graphite [117]. The second was CVD, such as the decomposition of a carbon source on metal substrates, for example, copper and nickel [118, 119]. The third was the epitaxial growth on electrically insulating surfaces, for example, SiC [120]. The fourth was the liquid-phase exfoliation of graphite into graphene nano-platelets [121].

The resulting graphene obtained by the above methods exhibit diversities in sample size and quality, implying their applicability for niche applications. Micromechanical exfoliation has, for example, yielded the highest quality but with small sample sizes ranging from few micrometers to ~1 mm, which are applicable only for fundamental studies on their transport properties. Large-area, uniform, and continuous graphene films are now achievable by CVD on Cu foil, but they exhibit moderate charge carrier mobility. A complete process requires the transfer from the Cu foil to a target substrate, and the production of square meters of graphene has already been achieved. The polymers used as a supporting

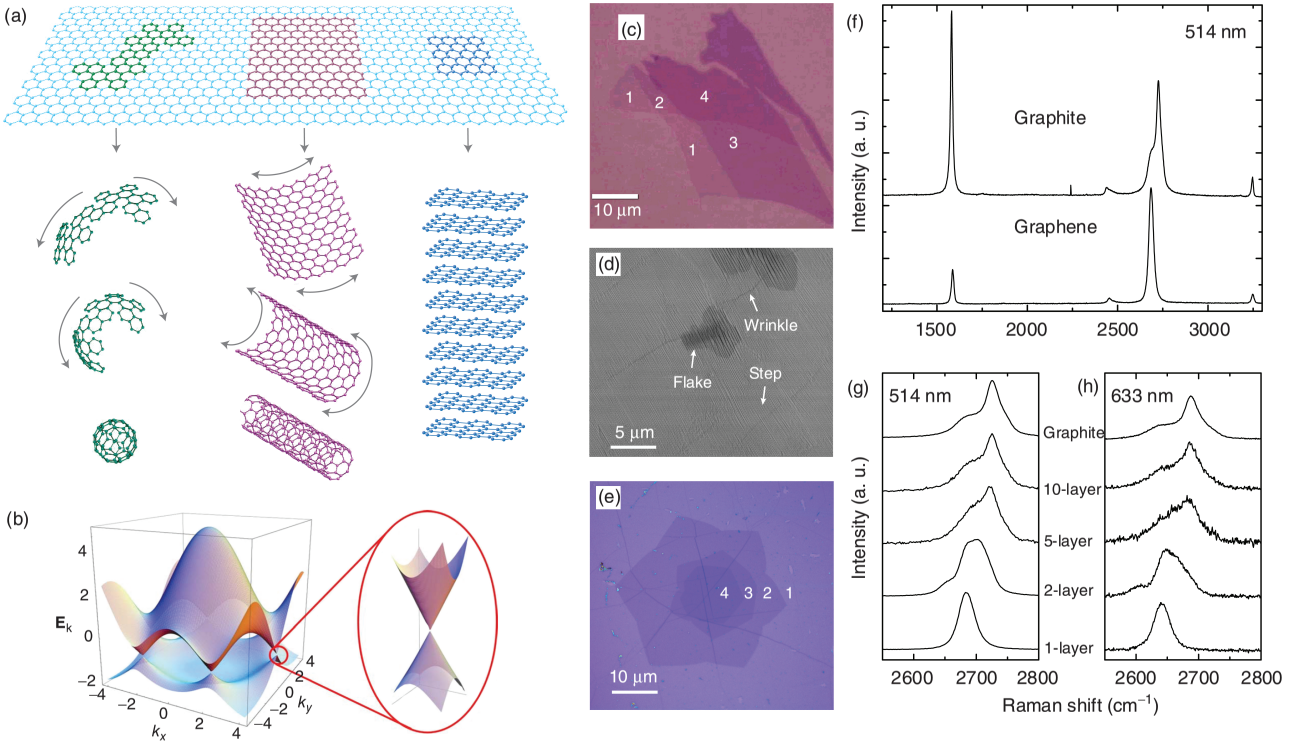

Figure 1.4 (a) Graphene is a 2D building material for carbon materials of all other dimensionalities. It can be wrapped up into 0D buckyballs, rolled into 1D nanotubes, or stacked into 3D graphite. (Reprinted with permission from [104]. ©2007 Nature Publishing Group.) (b) Electronic dispersion in the honeycomb lattice. Left: energy spectrum (in units of t) for finite values of t and t', with $t = 2.7$ eV and $t' = -0.2t$. Right: zoom-in of the energy bands close to one of the Dirac points. (Reprinted with permission from [105]. ©2009 American Physical Society.) Characterization of graphene. (c) Optical image of mechanically exfoliated graphene flakes with one, two, three, and four layers on a SiO_2(285 nm)-on-Si substrate. (Reprinted with permission from [106]. ©2007 American Chemical Society.) (d) High-resolution SEM and (e) optical images of CVD-grown graphene transferred on to a SiO_2(285 nm)-on-Si substrate, respectively. (f) Comparison of Raman spectra recorded at 514 nm for bulk graphite and graphene. The 2D peaks at 2700 cm^{-1} are scaled to have similar height; evolution of the spectra at (g) 514 nm (h) 633 nm with the number of layers. (Reprinted with permission from [107]. ©2006 American Physical Society.)

layer in the transferring procedure, however, are rather difficult to be completely removed from the graphene surface. The residual polymers are found to greatly influence the graphene's properties and thus make the materials properties less controllable in devices. CVD-grown graphene films are ready for use in transparent conductive coating applications, sensors, and nanoelectronics, although there are defects, grain boundaries, and thicker graphene that would result in variable device performance from one device to another. The quality of graphene grown on SiC can be very high, with crystallites approaching hundreds of micrometers in size. Thus, SiC-grown graphene may find application in high-frequency transistors. In the liquid exfoliation of graphite, intercalation of solvents into the gallery of graphite favors the interlayer expansion. With further aids of sonication and thermal or plasma processes, such graphite intercalated compounds can subsequently be delaminated into graphene nano-platelets, with a wide dispersion of thickness and lateral size, strongly depending on the treatment conditions [121]. The tone-scale synthesis of graphene via this method is currently being evaluated in numerous applications in printed electronics, electromagnetic shielding, barrier coatings, heat dissipation, supercapacitors, and so on [122].

The peculiar chemical and physical properties of graphene have demonstrated experimentally a strong dependence on the number of graphene layers, the quality of the material, the type of defects, and the substrates. In this context, it is of critical importance to perform various characterizations on graphene in order to explore the issues mentioned above. Optical microscopy is a quick and precise method to rapidly locate graphene and to determine the thickness of graphene nano-platelets in terms of their contrast spectrum. One can observe a contrast between the graphene layers and SiO_2(285 nm)/Si substrate in a reflection spectrum using a normal white-light illumination on samples supported on a substrate (Figure 1.4c) [106]. The graphene sample shows four different contrast regions, which are related to four different thicknesses. By fitting the experimental data to Fresnel's law, the experimental refractive index of a single-layer graphene $n = 2.0 - 1.1i$ differs from that of bulk graphite $n = 2.6 - 1.3i$ in the visible range. Such a large deviation was ascribed to the decrease of interlayer interaction in the ultrathin range. In similar cases, the thickness of few-layer graphene with less than 10 layers has clearly been discriminated. As to a continuous graphene film on a Cu foil by CVD, scanning electron microscopy (SEM) is an efficient method for the direct evaluation. Figure 1.4d depicts a higher resolution image of graphene on Cu with the presence of Cu surface steps, graphene "wrinkles," and the presence of nonuniform dark flakes. The wrinkles are caused by the thermal expansion coefficient difference between Cu and graphene. The CVD-grown graphene also exhibits a clear contrast between the graphene layers when it is transferred onto the SiO_2(285 nm)/Si substrate (Figure 1.4e).

Raman spectroscopy is another nondestructive and quick inspection method for evaluating the thickness and quality of graphene. In the Raman spectra of graphene, a G peak located at $\sim$1580 cm^{-1} and a 2D peak at $\sim$2700 cm^{-1} are observed, as shown in Figure 1.4f, corresponding to the in-plane optical vibration (degenerate zone-center E_{2g} mode) and second-order of zone-boundary phonons,

respectively [107]. The D peak, located at ~1350 cm^{-1} due to first-order zone boundary phonons, is absent from defect-free graphene. It will be activated by defects, vacancy, and structural disorder in graphene. The number of layers in graphene can be determined by the shape, width, and position of the 2D peak. Figure 1.4g and h shows that the 2D peak shifts to higher wavenumber values and becomes broader with an increase in the number of layers. For more than five layers, however, the Raman spectrum becomes hardly distinguishable from that of bulk graphite. Raman spectroscopy has also been useful in identifying the quality and types of edge, the effects of perturbations, such as electric and magnetic fields, strain, doping, disorder, and functional groups [123].

1.4.2 Functionalization of Graphene and Graphene Oxide

The chemical modification of graphene generally includes covalent attachment of organic molecules, hydrogen, and halogens to pristine graphene and/or its derivatives, noncovalent functionalization, and deposition of various nanoparticles on it [124].

Graphene and graphene oxide with large surface area, delocalized π electrons, and easy functionalization by various molecules provide opportunities for applications in nanodevices, energy-storage materials, and polymer composites [115]. In terms of the solid-state ^{13}C NMR spectroscopy analysis done to date (Figure 1.2a–c) [125, 126], the possible structural model of graphene oxide has been proposed in Figure 1.4d [126]. The carbon network is bonded to hydroxyl groups or epoxide groups as well as five- and six-membered lactols. Most of covalent functionalization methods rely on these groups that are active sites.

Covalent chemistry has proven to be an effective path to convert the sp^2-hybridized carbon atoms into sp^3-hybridized ones by forming a single bond with external groups. For example, the aryl radicals dissociated from diazonium salts upon heating broke the –C═C– double bonds and introduced aryl groups onto the graphene plane [127]. By use of photoinduced free radicals, one can also introduce aryl groups onto graphene scaffold from benzoyl peroxide. However, the free-radical reactions usually give rise to disordered crystal structures [128].

It would be ideal to control the crystal structure and chemical composition of graphene derivatives. Theoretical calculations predicted the existence of fully hydrogenated and fluorinated graphene from both sides, named as graphane and fluorographene, respectively [129–131]. Graphane and fluorographene are both thermodynamically stable with a C/H or C/F ratio of 1:1. Graphane has two stable configurations: a chair conformer and a boat conformer, the former being slightly more stable than the latter. The direct bandgap values at the K point are 3.5 and 3.7 eV for the former and latter, respectively. By exposing free-standing graphene to a hydrogen plasma, one can achieve the double-sided hydrogenation of graphene [132]. The electron diffraction (ED) pattern revealed that the graphane has a hexagonal symmetry with a lattice constant $d = 2.46 \pm 0.02$ Å, which is ~1% smaller than that of pristine graphene. This lattice shrinkage after exposure to H

radicals arises from the change of carbon configuration from sp^2 to sp^3, which generally results in longer C–C bonds. The unit cell of fluorographene is, in contrast, ~1% larger than that of graphene as a consequence of the corrugation [133], whereas the measured unit cell of C_2F chair, partially fluorinated graphene on one side, revealed a 2.4% expansion with respect to graphene, which is larger than corrugated fluorographene. The C_2F chair, one-sided fluorination of graphene, demonstrated a much higher degree of pristine long-range structural and morphological order than fluorographene [134]. The tetragonal "boat" form exhibits a short-range order.

Noncovalent functionalization involves the reactions with biocompatible polymers or biomolecules via hydrophobic interactions, $\pi-\pi$ stacking, or electrostatic interactions. Such modification greatly improves their stability in aqueous solutions. Since graphene oxide nanosheets are negatively charged, a positively charged polyelectrolyte (PEI) can effectively bind with them via electrostatic interactions. The resulting nano-graphene oxide (nGO)/PEI hybrids, for example, show much improved physiological stability compared to graphene oxide, reduced toxicity compared to bare PEI, and high gene transfection efficiency [135].

Deposition of nanoparticles, including those of metals (e.g., Au, Ag, Pd, Pt, Ni, and Cu) and metal oxides (TiO_2, ZnO, MnO_2, Co_3O_4, and Fe_3O_4), on graphene and nGO demonstrates the potential for their applications in biomedicine [136]. For example, graphene oxide/iron oxide nanoparticle composites have been investigated for magnetic targeted drug delivery and *in vivo* multimodal-imaging-guided photothermal therapy because of their interesting magnetic and optical properties.

Biofunctionalization of graphene and graphene oxide with biomolecules and cells have expanded their applications to a variety of biological platforms, biosensors, and biodevices. Until now, a number of biomolecules, for example, nucleic acids (NAs), peptides, proteins and cells, have been successfully employed in biological modification of graphene and graphene oxide (Figure 1.5a) [137]. One can also achieve its surface modification through reaction with various hydrophilic macromolecules, such as PEG (Figure 1.5b–f) [138], amine-modified dextran (DEX) [139], and poly(acrylic acid) (PAA) [140]. The modified graphene oxides have exhibited improved biocompatibility, reduced nonspecific binding to biological molecules and cells, and improved *in vivo* pharmacokinetics for better tumor targeting [138].

1.4.3 Prospects and Challenges

In more than 10 years of worldwide research, graphene and its derivatives with fascinating properties have shown potential for applications. Toward these applications, mass production techniques are required to produce uniform graphene nano-platelets. Low-temperature growth of large-area, uniform, high-quality bilayer and multilayer graphene films on arbitrary substrates need to be developed. The efficient, intact, and clean transfer from metal substrates

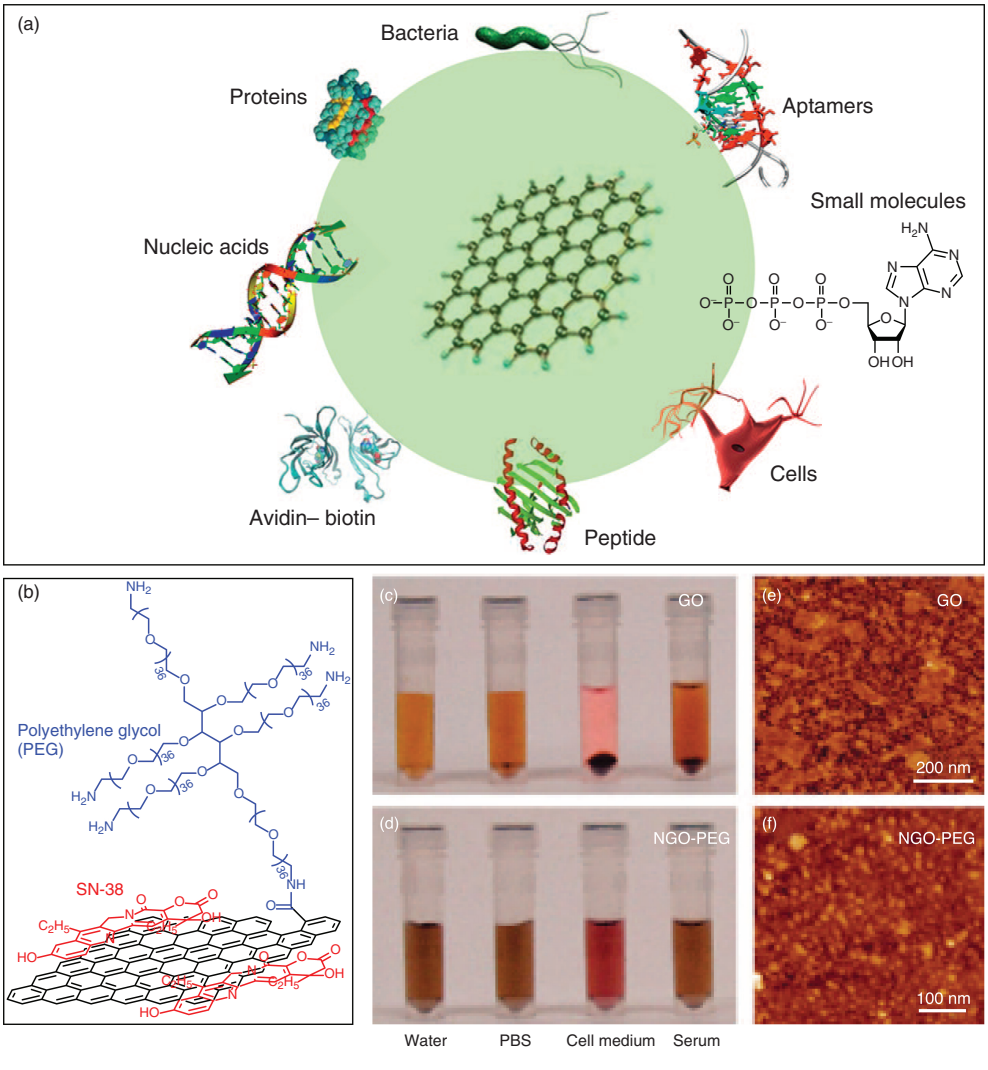

Figure 1.5 (a) Logo for biofunctionalization of graphene and its derivatives with avidin–biotin, peptides, nucleic acids, proteins, aptamers, small molecules, bacteria, and cells through physical adsorption or chemical conjugation. (Reprinted with permission from [137]. ©2011 Cell Press). Nano-graphene oxide (nGO)–PEG for drug loading and delivery. (b) Schematic structure of SN38 loading on nGO–PEG. PEGylation of graphene oxide: photos of (c) GO and (d) nGO–PEG in different solutions recorded after centrifugation at 10 000*g* for 5 min. GO crashed out slightly in PBS and completely in cell medium and serum (top panel). nGO–PEG was stable in all solutions. AFM images of (e) GO and (f) nGO–PEG. (Reprinted with permission from [138]. ©2008 American Society Chemistry.)

without etching the metals remains challenging. The combination of graphene and biotechnology is still in its infancy. There are many issues to be resolved before putting graphene to bioapplications. The potential long-term toxicity has been central to these issues. Whether and how graphene and its derivatives gradually degrade in biological system is essentially unclear. Its influence on the immune and reproductive systems of animals requires more research activities.

1.5 Summary and Outlook

In the past three decades, researchers all over the world have carried out extensive studies on carbon nanomaterials, especially fullerenes, CNTs, and graphene. Various methods to synthesize these nanomaterials with different morphology and structures have been reported. Diverse and attractive mechanical, chemical, and physical properties have also been investigated by means of state-of-the-art characterization tools. Based on these comprehensive studies, carbon nanomaterials are believed to have the potential for use in many exciting applications in many fields.

However, most of the proposed applications have not been realized. Till now, it is widely accepted that the biggest challenge to achieve these practical applications is obtaining enough amount of carbon nanomaterials having a designated structure. Researchers are now reconsidering ways to synthesize carbon nanomaterials.

The first thing is to set up effective methods to produce carbon nanomaterials with a precisely controlled structure and identical properties. The chirality, diameter, layer number, and even the assembly status of CNTs may change their optical, electrical, and biological behaviors dramatically. Similarly, the layer number, width, edge structure, and defect number of graphene determine its properties and feasible applications. Therefore, a uniform sample having the same structure is required for many real applications, especially in the electrical and biological fields.

The second consideration is the production yield. Now it is possible to synthesize or separate identical fullerene isomers and CNTs of a single chirality. Graphene ribbons in a narrow range of widths were also successfully engineered in the laboratory. The problem is that the obtained amount is far below that is needed for practical usage. It remains a big challenge to improve the yield of these materials with structural purity. On the other hand, researchers are currently able to produce CNTs and graphene on an industrial scale despite the precise control on their fine structures, which greatly promote the progress toward some applications such as films, composites, and surface coating. In this aspect, it will be very helpful to further decrease the production cost and keep a comparatively high structural quality at the same time.

In conclusion, to achieve practical applications, the primary goal and task is to scale up the production of carbon nanomaterials in a reproducible way, preferably with a precise control on their fine structures.

References

1. Heath, J.R., Zhang, Q., O'Brien, S.C., Curl, R.F., Kroto, H.W., and Smalley, R.E. (1987) The formation of long carbon chain molecules during laser vaporization of graphite. *J. Am. Chem. Soc.*, **109**, 359–363.
2. Heath, J.R., O'Brien, S.C., Zhang, Q., Liu, Y., Curl, R.F., Tittel, F.K., and Smalley, R.E. (1985) Lanthanum complexes of spheroidal carbon shells. *J. Am. Chem. Soc.*, **107**, 7779–7780.
3. Chai, Y., Guo, T., Jin, C., Haufler, R.E., Chibante, L.P.F., Fure, J., Wang, L., Alford, J.M., and Smalley, R.E. (1991) Fullerenes with metals inside. *J. Phys. Chem.*, **95**, 7564–7568.
4. Stevenson, S., Rice, G., Glass, T., Harich, K., Cromer, F., Jordan, M.R., Craft, J., Hadju, E., Bible, R., Olmstead, M.M., Maitra, K., Fisher, A.J., Balch, A.L., and Dorn, H.C. (1999) Small-bandgap endohedral metallofullerenes in high yield and purity. *Nature*, **401**, 55–57.
5. Yang, S., Zhang, L., Zhang, W., and Dunsch, L. (2010) A facile route to metal nitride clusterfullerenes by using guanidinium salts: a selective organic solid as the nitrogen source. *Chem. Eur. J.*, **16**, 12398–12405.
6. Mercado, B.Q., Olmstead, M.M., Beavers, C.M., Easterling, M.L., Stevenson, S., Mackey, M.A., Coumbe, C.E., Phillips, J.D., Phillips, J.P., Poblet, J.M., and Balch, A.L. (2010) A seven atom cluster in a carbon cage, the crystallographically determined structure of Sc4([small mu]3-O)3@Ih-C80. *Chem. Commun.*, **46**, 279–281.
7. Chen, N., Chaur, M.N., Moore, C., Pinzon, J.R., Valencia, R., Rodriguez-Fortea, A., Poblet, J.M., and Echegoyen, L. (2010) Synthesis of a new endohedral fullerene family, Sc2S@C2n (n = 40-50) by the introduction of SO2. *Chem. Commun.*, **46**, 4818–4820.
8. Lu, X., Shi, Z.J., Sun, B.Y., He, X.R., and Gu, Z.N. (2005) Isolation and spectroscopic study of a series of monogadolinium endohedral metallofullerenes. *Fullerenes Nanotubes Carbon Nanostruct.*, **13**, 13–20.
9. Feng, L., Sun, B.Y., He, X.R., and Gu, Z.N. (2002) Isolation and spectroscopic study of a series of monoterbium endohedral metallofullerenes. *Fullerenes Nanotubes Carbon Nanostruct.*, **10**, 353–361.
10. Akasaka, T., Okubo, S., Kondo, M., Maeda, Y., Wakahara, T., Kato, T., Suzuki, T., Yamamoto, K., Kobayashi, K., and Nagase, S. (2000) Isolation and characterization of two Pr@C82 isomers. *Chem. Phys. Lett.*, **319**, 153–156.
11. Diener, M.D. and Alford, J.M. (1998) Isolation and properties of small-bandgap fullerenes. *Nature*, **393**, 668–671.
12. Wakahara, T., Nikawa, H., Kikuchi, T., Nakahodo, T., Rahman, G.M.A., Tsuchiya, T., Maeda, Y., Akasaka, T., Yoza, K., Horn, E., Yamamoto, K., Mizorogi, N., Slanina, Z., and Nagase, S. (2006) La@C72 having a non-IPR carbon cage. *J. Am. Chem. Soc.*, **128**, 14228–14229.
13. Nikawa, H., Kikuchi, T., Wakahara, T., Nakahodo, T., Tsuchiya, T., Rahman, G.M.A., Akasaka, T., Maeda, Y., Yoza, K., Horn, E., Yamamoto, K., Mizorogi, N., and Nagase, S. (2005) Missing metallofullerene La@C74. *J. Am. Chem. Soc.*, **127**, 9684–9685.
14. Nikawa, H., Yamada, T., Cao, B.P., Mizorogi, N., Slanina, Z., Tsuchiya, T., Akasaka, T., Yoza, K., and Nagase, S. (2009) Missing metallofullerene with C80 cage. *J. Am. Chem. Soc.*, **131**, 10950–10954.
15. Akasaka, T., Lu, X., Kuga, H., Nikawa, H., Mizorogi, N., Slanina, Z., Tsuchiya, T., Yoza, K., and Nagase, S. (2010) Dichlorophenyl derivatives of La@C3v(7)-C82: endohedral metal induced localization of pyramidalization and spin on a triple-hexagon junction. *Angew. Chem. Int. Ed.*, **49**, 9715–9719.
16. Chaur, M.N., Melin, F., Ashby, J., Elliott, B., Kumbhar, A., Rao, A.M., and Echegoyen, L. (2008) Lanthanum nitride endohedral fullerenes

$La_3N@C_{2n}$ (43 <= n <= 55): preferential formation of $La_3N@C_{96}$. *Chem. Eur. J.*, **14**, 8213–8219.

17. Shinohara, H., Yamaguchi, H., Hayashi, N., Sato, H., Ohkohchi, M., Ando, Y., and Saito, Y. (1993) Isolation and spectroscopic properties of scandium fullerenes (Sc2@C74, Sc2@C82, and Sc2@C84). *J. Phys. Chem.*, **97**, 4259–4261.
18. Klute, R.C., Dorn, H.C., and McNair, H.M. (1992) HPLC separation of higher (C84+) fullerenes. *J. Chromatogr. Sci.*, **30**, 438–442.
19. Meier, M.S. and Selegue, J.P. (1992) Efficient preparative separation of C60 and C70. Gel permeation chromatography of fullerenes using 100% toluene as mobile phase. *J. Org. Chem.*, **57**, 1924–1926.
20. Bolskar, R.D. and Alford, J.M. (2003) Chemical oxidation of endohedral metallofullerenes: identification and separation of distinct classes. *Chem. Commun.*, 1292–1293.
21. Stevenson, S., Harich, K., Yu, H., Stephen, R.R., Heaps, D., Coumbe, C., and Phillips, J.P. (2006) Nonchromatographic "Stir and Filter Approach" (SAFA) for isolating Sc3N@C80 metallofullerenes. *J. Am. Chem. Soc.*, **128**, 8829–8835.
22. Stevenson, S., Mackey, M.A., Coumbe, C.E., Phillips, J.P., Elliott, B., and Echegoyen, L. (2007) Rapid removal of D5h isomer using the "stir and filter approach" and isolation of large quantities of isomerically pure Sc3N@C80 metallic nitride fullerenes. *J. Am. Chem. Soc.*, **129**, 6072–6073.
23. Lu, X., Feng, L., Akasaka, T., and Nagase, S. (2012) Current status and future developments of endohedral metallofullerenes. *Chem. Soc. Rev.*, **41**, 7723–7760.
24. Yamada, M., Someya, C., Wakahara, T., Tsuchiya, T., Maeda, Y., Akasaka, T., Yoza, K., Horn, E., Liu, M.T.H., Mizorogi, O.N., and Nagase, S. (2008) Metal atoms collinear with the spiro carbon of 6,6-open adducts, M2@C80(Ad) (M = La and Ce, Ad = adamantylidene). *J. Am. Chem. Soc.*, **130**, 1171–1176.
25. Xie, Y., Suzuki, M., Cai, W., Mizorogi, N., Nagase, S., Akasaka, T., and Lu, X. (2013) Highly regioselective addition of adamantylidene carbene to Yb@C2v(3)-C80 to afford the first derivative of divalent metallofullerenes. *Angew. Chem. Int. Ed.*, **52**, 5142–5145.
26. Zhang, W., Suzuki, M., Xie, Y., Bao, L., Cai, W., Slanina, Z., Nagase, S., Xu, M., Akasaka, T., and Lu, X. (2013) Molecular structure and chemical property of a divalent metallofullerene Yb@C2(13)-C84. *J. Am. Chem. Soc.*, **135**, 12730–12735.
27. Feng, L., Wakahara, T., Nakahodo, T., Tsuchiya, T., Piao, Q., Maeda, Y., Lian, Y., Akasaka, T., Horn, E., Yoza, K., Kato, T., Mizorogi, N., and Nagase, S. (2006) The Bingel monoadducts of La@C82: synthesis, characterization, and electrochemistry. *Chem. Eur. J.*, **12**, 5578–5586.
28. Yamada, M., Wakahara, T., Nakahodo, T., Tsuchiya, T., Maeda, Y., Akasaka, T., Yoza, K., Horn, E., Mizorogi, N., and Nagase, S. (2006) Synthesis and structural characterization of endohedral pyrrolidinodimetallofullerene: La2@C80(CH2)2NTrt. *J. Am. Chem. Soc.*, **128**, 1402–1403.
29. Akasaka, T., Kato, T., Kobayashi, K., Nagase, S., Yamamoto, K., Funasaka, H., and Takahashi, T. (1995) Exohedral adducts of La@C82. *Nature*, **374**, 600–601.
30. Popov, A.A., Yang, S., and Dunsch, L. (2013) Endohedral fullerenes. *Chem. Rev.*, **113**, 5989–6113.
31. Maeda, Y., Sato, S., Inada, K., Nikawa, H., Yamada, M., Mizorogi, N., Hasegawa, T., Tsuchiya, T., Akasaka, T., Kato, T., Slanina, Z., and Nagase, S. (2010) Regioselective exohedral functionalization of La@C82 and its 1,2,3,4,5-pentamethylcyclopentadiene and adamantylidene adducts. *Chem. Eur. J.*, **16**, 2193–2197.
32. Lu, X., Nikawa, H., Tsuchiya, T., Akasaka, T., Toki, M., Sawa, H., Mizorogi, N., and Nagase, S. (2010) Nitrated benzyne derivatives of La@C82: addition of NO2 and its

positional directing effect on the subsequent addition of benzynes. *Angew. Chem. Int. Ed.*, **49**, 594–597.

33. Takano, Y., Yomogida, A., Nikawa, H., Yamada, M., Wakahara, T., Tsuchiya, T., Ishitsuka, M.O., Maeda, Y., Akasaka, T., Kato, T., Slanina, Z., Mizorogi, N., and Nagase, S. (2008) Radical coupling reaction of paramagnetic endohedral metallofullerene La@C82. *J. Am. Chem. Soc.*, **130**, 16224–16230.
34. Shu, C., Slebodnick, C., Xu, L., Champion, H., Fuhrer, T., Cai, T., Reid, J.E., Fu, W., Harich, K., Dorn, H.C., and Gibson, H.W. (2008) Highly regioselective derivatization of trimetallic nitride templated endohedral metallofullerenes via a facile photochemical reaction. *J. Am. Chem. Soc.*, **130**, 17755–17760.
35. Fang, H., Cong, H., Suzuki, M., Bao, L., Yu, B., Xie, Y., Mizorogi, N., Olmstead, M.M., Balch, A.L., Nagase, S., Akasaka, T., and Lu, X. (2014) Regioselective benzyl radical addition to an open-shell cluster metallofullerene. Crystallographic studies of cocrystallized Sc3C2@Ih-C80 and its singly bonded derivative. *J. Am. Chem. Soc.*, **136**, 10534–10540.
36. Tsuchiya, T., Kurihara, H., Sato, K., Wakahara, T., Akasaka, T., Shimizu, T., Kamigata, N., Mizorogi, N., and Nagase, S. (2006) Supramolecular complexes of La@C82 with unsaturated thiacrown ethers. *Chem. Commun.*, 3585–3587.
37. Tsuchiya, T., Sato, K., Kurihara, H., Wakahara, T., Maeda, Y., Akasaka, T., Ohkubo, K., Fukuzumi, S., Kato, T., and Nagase, S. (2006) Spin-site exchange system constructed from endohedral metallofullerenes and organic donors. *J. Am. Chem. Soc.*, **128**, 14418–14419.
38. Takata, M., Umeda, B., Nishibori, E., Sakata, M., Saito, Y., Ohno, M., and Shinohara, H. (1995) Confirmation by X-ray diffraction of the endohedral nature of the metallofullerene Y@C_{82}. *Nature*, **377**, 46–49.
39. Nishibori, E., Ishihara, M., Takata, M., Sakata, M., Ito, Y., Inoue, T., and Shinohara, H. (2006) Bent (metal)2C2 clusters encapsulated in (Sc2C2)@C82(III) and (Y2C2)@C82(III) metallofullerenes. *Chem. Phys. Lett.*, **433**, 120–124.
40. Nishibori, E., Takata, M., Sakata, M., Inakuma, M., and Shinohara, H. (1998) Determination of the cage structure of Sc@C82 by synchrotron powder diffraction. *Chem. Phys. Lett.*, **298**, 79–84.
41. Nishibori, E., Takata, M., Sakata, M., Tanaka, H., Hasegawa, M., and Shinohara, H. (2000) Giant motion of La atom inside C82 cage. *Chem. Phys. Lett.*, **330**, 497–502.
42. Nishibori, E., Terauchi, I., Sakata, M., Takata, M., Ito, Y., Sugai, T., and Shinohara, H. (2006) High-resolution analysis of (Sc3C2)@C80 metallofullerene by third generation synchrotron radiation X-ray powder diffraction. *J. Phys. Chem. B*, **110**, 19215–19219.
43. Sun, B.Y., Sugai, T., Nishibori, E., Iwata, K., Sakata, M., Takata, M., and Shinohara, H. (2005) An anomalous endohedral structure of Eu@C82 metallofullerenes. *Angew. Chem. Int. Ed.*, **44**, 4568–4571.
44. Tsuchiya, T., Wakahara, T., Maeda, Y., Akasaka, T., Waelchli, M., Kato, T., Okubo, H., Mizorogi, N., Kobayashi, K., and Nagase, S. (2005) 2D NMR characterization of the La@C82 anion. *Angew. Chem. Int. Ed.*, **44**, 3282–3285.
45. Yamada, M., Wakahara, T., Lian, Y.F., Tsuchiya, T., Akasaka, T., Waelchli, M., Mizorogi, N., Nagase, S., and Kadish, K.M. (2006) Analysis of lanthanide-induced NMR shifts of the Ce@C82 anion. *J. Am. Chem. Soc.*, **128**, 1400–1401.
46. Kurihara, H., Lu, X., Iiduka, Y., Mizorogi, N., Slanina, Z., Tsuchiya, T., Akasaka, T., and Nagase, S. (2011) Sc_2C_2@C_{80} rather than Sc_2@C_{82}: templated formation of unexpected $C_{2v}(5)$-C_{80} and temperature-dependent dynamic motion of internal Sc_2C_2 cluster. *J. Am. Chem. Soc.*, **133**, 2382–2385.
47. Lu, X., Nakajima, K., Iiduka, Y., Nikawa, H., Mizorogi, N., Slanina, Z., Tsuchiya, T., Nagase, S., and Akasaka, T. (2011) Structural elucidation and regioselective functionalization of an unexplored carbide cluster metallofullerene

$Sc_2C_2@C_s(6)$-C_{82}. *J. Am. Chem. Soc.*, **133**, 19553–19558.

48. Lu, X., Nakajima, K., Iiduka, Y., Nikawa, H., Tsuchiya, T., Mizorogi, N., Slanina, Z., Nagase, S., and Akasaka, T. (2012) The long-believed $Sc_2@C_{2v}(17)$-C_{84} is actually $Sc_2C_2@C_{2v}(9)$-C_{82}: unambiguous structure assignment and chemical functionalization. *Angew. Chem. Int. Ed.*, **51**, 5889–5892.
49. Iiduka, Y., Wakahara, T., Nakajima, K., Tsuchiya, T., Nakahodo, T., Maeda, Y., Akasaka, T., Mizorogi, N., and Nagase, S. (2006) 13C NMR spectroscopic study of scandium dimetallofullerene, Sc2@C84 vs. Sc2C2@C82. *Chem. Commun. (Camb.)*, 2057–2059.
50. Akasaka, T., Nagase, S., Kobayashi, K., Walchli, M., Yamamoto, K., Funasaka, H., Kako, M., Hoshino, T., and Erata, T. (1997) ^{13}C and ^{139}La NMR studies of $La_2@C_{80}$: first evidence for circular motion of metal atoms in endohedral dimetallofullerenes. *Angew. Chem. Int. Ed. Engl.*, **36**, 1643–1645.
51. Lu, X., Akasaka, T., and Nagase, S. (2013) Carbide cluster metallofullerenes: structure, properties, and possible origin. *Acc. Chem. Res.*, **46**, 1627–1635.
52. Xu, W., Feng, L., Calvaresi, M., Liu, J., Liu, Y., Niu, B., Shi, Z., Lian, Y., and Zerbetto, F. (2013) An experimentally observed trimetallofullerene Sm-3@I-h-C-80: encapsulation of three metal atoms in a cage without a nonmetallic mediator. *J. Am. Chem. Soc.*, **135**, 4187–4190.
53. Kobayashi, K. and Nagase, S. (2002) A stable unconventional structure of Sc2@C66 found by density functional calculations. *Chem. Phys. Lett.*, **362**, 373–379.
54. Lee, H.M., Olmstead, M.M., Suetsuna, T., Shimotani, H., Dragoe, N., Cross, R.J., Kitazawa, K., and Balch, A.L. (2002) Crystallographic characterization of Kr@C60 in (0.09Kr@C60/0.91C60)·{NiII(OEP)}·2C6H6. *Chem. Commun.*, 1352–1353.
55. Che, Y., Yang, H., Wang, Z., Jin, H., Liu, Z., Lu, C., Zuo, T., Dorn, H.C., Beavers, C.M., Olmstead, M.M., and Balch, A.L. (2009) Isolation and structural characterization of two very large, and largely empty, endohedral fullerenes: Tm@C(3v)-C(94) and Ca@C(3v)-C(94). *Inorg. Chem.*, **48**, 6004–6010.
56. Yang, H., Jin, H., Zhen, H., Wang, Z., Liu, Z., Beavers, C.M., Mercado, B.Q., Olmstead, M.M., and Balch, A.L. (2011) Isolation and crystallographic identification of four isomers of Sm@C90. *J. Am. Chem. Soc.*, **133**, 6299–6306.
57. Aoyagi, S., Nishibori, E., Sawa, H., Sugimoto, K., Takata, M., Miyata, Y., Kitaura, R., Shinohara, H., Okada, H., Sakai, T., Ono, Y., Kawachi, K., Yokoo, K., Ono, S., Omote, K., Kasama, Y., Ishikawa, S., Komuro, T., and Tobita, H. (2010) A layered ionic crystal of polar Li@C60 superatoms. *Nat. Chem.*, **2**, 678–683.
58. Hernandez-Eguia, L.P., Escudero-Adan, E.C., Pinzon, J.R., Echegoyen, L., and Ballester, P. (2011) Complexation of Sc3N@C80 endohedral fullerene with cyclic Zn-bisporphyrins: solid state and solution studies. *J. Org. Chem.*, **76**, 3258–3265.
59. Dresselhaus, M.S., Dresselhaus, G., and Jorio, A. (2004) Unusual properties and structure of carbon nanotubes. *Annu. Rev. Mater. Res.*, **34**, 247–278.
60. Iijima, S. (1991) Helical microtubules of graphitic carbon. *Nature*, **354**, 56–58.
61. Iijima, S. and Ichihashi, T. (1993) Single-shell carbon nanotubes of 1-nm diameter. *Nature*, **363**, 603–605.
62. Byrne, M.T. and Gun'ko, Y.K. (2010) Recent advances in research on carbon nanotube-polymer composites. *Adv. Mater.*, **22**, 1672–1688.
63. Spitalsky, Z., Tasis, D., Papagelis, K., and Galiotis, C. (2010) Carbon nanotube-polymer composites: chemistry, processing, mechanical and electrical properties. *Prog. Polym. Sci.*, **35**, 357–401.
64. McCarthy, M.A., Liu, B., Donoghue, E.P., Kravchenko, I., Kim, D.Y., So, F., and Rinzler, A.G. (2011) Low-voltage, low-power, organic light-emitting transistors for active matrix displays. *Science*, **332**, 570–573.
65. Che, Y.C., Chen, H.T., Gui, H., Liu, J., Liu, B.L., and Zhou, C.W. (2014)

Review of carbon nanotube nanoelectronics and macroelectronics. *Semicond. Sci. Technol.*, **29**, 073001.

66. Wilson, N.R. and Macpherson, J.V. (2009) Carbon nanotube tips for atomic force microscopy. *Nat. Nanotechnol.*, **4**, 483–491.
67. Wang, J., Hu, Z., Xu, J.X., and Zhao, Y.L. (2014) Therapeutic applications of low-toxicity spherical nanocarbon materials. *NPG Asia Mater.*, **6**, e84.
68. Bethune, D.S., Kiang, C.H., Devries, M.S., Gorman, G., Savoy, R., Vazquez, J., and Beyers, R. (1993) Cobalt-catalyzed growth of carbon nanotubes with single-atomic-layerwalls. *Nature*, **363**, 605–607.
69. Journet, C., Maser, W.K., Bernier, P., Loiseau, A., de la Chapelle, M.L., Lefrant, S., Deniard, P., Lee, R., and Fischer, J.E. (1997) Large-scale production of single-walled carbon nanotubes by the electric-arc technique. *Nature*, **388**, 756–758.
70. Guo, T., Nikolaev, P., Rinzler, A.G., Tomanek, D., Colbert, D.T., and Smalley, R.E. (1995) Self-assembly of tubular fullerenes. *J. Phys. Chem.*, **99**, 10694–10697.
71. Thess, A., Lee, R., Nikolaev, P., Dai, H.J., Petit, P., Robert, J., Xu, C.H., Lee, Y.H., Kim, S.G., Rinzler, A.G., Colbert, D.T., Scuseria, G.E., Tomanek, D., Fischer, J.E., and Smalley, R.E. (1996) Crystalline ropes of metallic carbon nanotubes. *Science*, **273**, 483–487.
72. Iijima, S., Yudasaka, M., Yamada, R., Bandow, S., Suenaga, K., Kokai, F., and Takahashi, K. (1999) Nano-aggregates of single-walled graphitic carbon nanohorns. *Chem. Phys. Lett.*, **309**, 165–170.
73. Azami, T., Kasuya, D., Yuge, R., Yudasaka, M., Iijima, S., Yoshitake, T., and Kubo, Y. (2008) Large-scale production of single-wall carbon nanohorns with high purity. *J. Phys. Chem. C*, **112**, 1330–1334.
74. Dai, J.Y., Lauerhaas, J.M., Setlur, A.A., and Chang, R.P.H. (1996) Synthesis of carbon-encapsulated nanowires using polycyclic aromatic hydrocarbon precursors. *Chem. Phys. Lett.*, **258**, 547–553.
75. Kong, J., Cassell, A.M., and Dai, H.J. (1998) Chemical vapor deposition of methane for single-walled carbon nanotubes. *Chem. Phys. Lett.*, **292**, 567–574.
76. Li, Y., Liu, J., Wang, Y.Q., and Wang, Z.L. (2001) Preparation of monodispersed Fe-Mo nanoparticles as the catalyst for CVD synthesis of carbon nanotubes. *Chem. Mater.*, **13**, 1008–1014.
77. Zheng, B., Lu, C.G., Gu, G., Makarovski, A., Finkelstein, G., and Liu, J. (2002) Efficient CVD growth of single-walled carbon nanotubes on surfaces using carbon monoxide precursor. *Nano Lett.*, **2**, 895–898.
78. Huang, S.M., Cai, X.Y., and Liu, J. (2003) Growth of millimeter-long and horizontally aligned single-walled carbon nanotubes on flat substrates. *J. Am. Chem. Soc.*, **125**, 5636–5637.
79. Hata, K., Futaba, D.N., Mizuno, K., Namai, T., Yumura, M., and Iijima, S. (2004) Water-assisted highly efficient synthesis of impurity-free single-waited carbon nanotubes. *Science*, **306**, 1362–1364.
80. Liu, Z.F., Jiao, L.Y., Yao, Y.G., Xian, X.J., and Zhang, J. (2010) Aligned, ultralong single-walled carbon nanotubes: from synthesis, sorting, to electronic devices. *Adv. Mater.*, **22**, 2285–2310.
81. Jiang, K.L., Wang, J.P., Li, Q.Q., Liu, L.A., Liu, C.H., and Fan, S.S. (2011) Superaligned carbon nanotube arrays, films, and yarns: a road to applications. *Adv. Mater.*, **23**, 1154–1161.
82. Harutyunyan, A.R., Chen, G.G., Paronyan, T.M., Pigos, E.M., Kuznetsov, O.A., Hewaparakrama, K., Kim, S.M., Zakharov, D., Stach, E.A., and Sumanasekera, G.U. (2009) Preferential growth of single-walled carbon nanotubes with metallic conductivity. *Science*, **326**, 116–120.
83. Wang, H., Wei, L., Ren, F., Wang, Q., Pfefferle, L.D., Haller, G.L., and Chen, Y. (2013) Chiral-selective CoSO4/SiO2 catalyst for (9,8) single-walled carbon nanotube growth. *ACS Nano*, **7**, 614–626.
84. Yang, F., Wang, X., Zhang, D.Q., Yang, J., Luo, D., Xu, Z.W., Wei, J.K., Wang,

J.Q., Xu, Z., Peng, F., Li, X.M., Li, R.M., Li, Y.L., Li, M.H., Bai, X.D., Ding, F., and Li, Y. (2014) Chirality-specific growth of single-walled carbon nanotubes on solid alloy catalysts. *Nature*, **510**, 522524.

85. Tasis, D., Tagmatarchis, N., Bianco, A., and Prato, M. (2006) Chemistry of carbon nanotubes. *Chem. Rev.*, **106**, 1105–1136.
86. Niyogi, S., Hamon, M.A., Hu, H., Zhao, B., Bhowmik, P., Sen, R., Itkis, M.E., and Haddon, R.C. (2002) Chemistry of single-walled carbon nanotubes. *Acc. Chem. Res.*, **35**, 1105–1113.
87. Wenseleers, W., Vlasov, I.I., Goovaerts, E., Obraztsova, E.D., Lobach, A.S., and Bouwen, A. (2004) Efficient isolation and solubilization of pristine single-walled nanotubes in bile salt micelles. *Adv. Funct. Mater.*, **14**, 1105–1112.
88. Gubitosi, M., Trilo, J.V., Vargas, A.A., Pavel, N.V., Gazzoli, D., Sennato, S., Jover, A., Meijide, F., and Galantini, L. (2014) Characterization of carbon nanotube dispersions in solutions of bile salts and derivatives containing aromatic substituents. *J. Phys. Chem. B*, **118**, 1012–1021.
89. Zheng, M., Jagota, A., Semke, E.D., Diner, B.A., Mclean, R.S., Lustig, S.R., Richardson, R.E., and Tassi, N.G. (2003) DNA-assisted dispersion and separation of carbon nanotubes. *Nat. Mater.*, **2**, 338–342.
90. Tu, X.M., Manohar, S., Jagota, A., and Zheng, M. (2009) DNA sequence motifs for structure-specific recognition and separation of carbon nanotubes. *Nature*, **460**, 250–253.
91. Geng, J., Kim, K., Zhang, J.F., Escalada, A., Tunuguntla, R., Comolli, L.R., Allen, F.I., Shnyrova, A.V., Cho, K.R., Munoz, D., Wang, Y.M., Grigoropoulos, C.P., Ajo-Franklin, C.M., Frolov, V.A., and Noy, A. (2014) Stochastic transport through carbon nanotubes in lipid bilayers and live cell membranes. *Nature*, **514**, 612615.
92. Bottini, M., Rosato, N., and Bottini, N. (2011) PEG-modified carbon nanotubes in biomedicine: current status and challenges ahead. *Biomacromolecules*, **12**, 3381–3393.
93. Liu, Z., Tabakman, S.M., Chen, Z., and Dai, H.J. (2009) Preparation of carbon nanotube bioconjugates for biomedical applications. *Nat. Protoc.*, **4**, 1372–1382.
94. Matsumura, S., Sato, S., Yudasaka, M., Tomida, A., Tsruruo, T., Iijima, S., and Shiba, K. (2009) Prevention of carbon nanohorn agglomeration using a conjugate composed of comb-shaped polyethylene glycol and a peptide aptamer. *Mol. Pharmaceutics*, **6**, 441–447.
95. Xu, J.X., Iijima, S., and Yudasaka, M. (2010) Appropriate PEG compounds for dispersion of single wall carbon nanohorns in salted aqueous solution. *Appl. Phys. A*, **99**, 15–21.
96. Suenaga, K., Wakabayashi, H., Koshino, M., Sato, Y., Urita, K., and Iijima, S. (2007) Imaging active topological defects in carbon nanotubes. *Nat. Nanotechnol.*, **2**, 358–360.
97. Suenaga, K. and Koshino, M. (2010) Atom-by-atom spectroscopy at graphene edge. *Nature*, **468**, 1088–1090.
98. Ge, C.C., Du, J.F., Zhao, L.N., Wang, L.M., Liu, Y., Li, D.H., Yang, Y.L., Zhou, R.H., Zhao, Y.L., Chai, Z.F., and Chen, C.Y. (2011) Binding of blood proteins to carbon nanotubes reduces cytotoxicity. *Proc. Natl. Acad. Sci. U.S.A.*, **108**, 16968–16973.
99. Hartschuh, A. (2008) Tip-enhanced near-field optical microscopy. *Angew. Chem. Int. Ed.*, **47**, 8178–8191.
100. Nakayama, T., Kubo, O., Shingaya, Y., Higuchi, S., Hasegawa, T., Jiang, C.S., Okuda, T., Kuwahara, Y., Takami, K., and Aono, M. (2012) Development and application of multiple-probe scanning probe microscopes. *Adv. Mater.*, **24**, 1675–1692.
101. Dresselhaus, M.S., Jorio, A., Hofmann, M., Dresselhaus, G., and Saito, R. (2010) Perspectives on carbon nanotubes and graphene Raman spectroscopy. *Nano Lett.*, **10**, 751–758.
102. Dresselhaus, M.S., Jorio, A., and Saito, R. (2010) Characterizing graphene, graphite, and carbon nanotubes by Raman spectroscopy. *Annu. Rev. Condens. Matter Phys.*, **1**, 89–108.

103. Fagan, J.A., Bauer, B.J., Hobbie, E.K., Becker, M.L., Walker, A.R.H., Simpson, J.R., Chun, J., Obrzut, J., Bajpai, V., Phelan, F.R., Simien, D., Huh, J.Y., and Migler, K.B. (2011) Carbon nanotubes: measuring dispersion and length. *Adv. Mater.*, **23**, 338–348.

104. Geim, A.K. and Novoselov, K.S. (2007) The rise of graphene. *Nat. Mater.*, **6**, 183–191.

105. Castro Neto, A.H., Guinea, F., Peres, N.M.R., Novoselov, K.S., and Geim, A.K. (2009) The electronic properties of graphene. *Rev. Mod. Phys.*, **81**, 109–162.

106. Ni, Z.H., Wang, H.M., Kasim, J., Fan, H.M., Yu, T., Wu, Y.H., Feng, Y.P., and Shen, Z.X. (2007) Graphene thickness determination using reflection and contrast spectroscopy. *Nano Lett.*, **7**, 2758–2763.

107. Ferrari, A.C., Meyer, J.C., Scardaci, V., Casiraghi, C., Lazzeri, M., Mauri, F., Piscanec, S., Jiang, D., Novoselov, K.S., Roth, S., and Geim, A.K. (2006) Raman spectrum of graphene and graphene layers. *Phys. Rev. Lett.*, **97**, 187401.

108. Bolotin, K.I., Sikes, K.J., Jiang, Z., Klima, M., Fudenberg, G., Hone, J., Kim, P., and Stormer, H.L. (2008) Ultrahigh electron mobility in suspended graphene. *Solid State Commun.*, **146**, 351–355.

109. Morozov, S.V., Novoselov, K.S., Katsnelson, M.I., Schedin, F., Elias, D.C., Jaszczak, J.A., and Geim, A.K. (2008) Giant intrinsic carrier mobilities in graphene and its bilayer. *Phys. Rev. Lett.*, **100**, 016602.

110. Lee, C., Wei, X.D., Kysar, J.W., and Hone, J. (2008) Measurement of the elastic properties and intrinsic strength of monolayer graphene. *Science*, **321**, 385–388.

111. Nair, R.R., Blake, P., Grigorenko, A.N., Novoselov, K.S., Booth, T.J., Stauber, T., Peres, N.M.R., and Geim, A.K. (2008) Fine structure constant defines visual transparency of graphene. *Science*, **320**, 1308.

112. Balandin, A.A., Ghosh, S., Bao, W.Z., Calizo, I., Teweldebrhan, D., Miao, F., and Lau, C.N. (2008) Superior thermal conductivity of single-layer graphene. *Nano Lett.*, **8**, 902–907.

113. Novoselov, K.S., Geim, A.K., Morozov, S.V., Jiang, D., Zhang, Y., Dubonos, S.V., Grigorieva, I.V., and Firsov, A.A. (2004) Electric field effect in atomically thin carbon films. *Science*, **306**, 666–669.

114. Zhang, Y.B., Tan, Y.W., Stormer, H.L., and Kim, P. (2005) Experimental observation of the quantum Hall effect and Berry's phase in graphene. *Nature*, **438**, 201–204.

115. Dreyer, D.R., Park, S., Bielawski, C.W., and Ruoff, R.S. (2010) The chemistry of graphene oxide. *Chem. Soc. Rev.*, **39**, 228–240.

116. Zhu, Y.W., Murali, S., Cai, W.W., Li, X.S., Suk, J.W., Potts, J.R., and Ruoff, R.S. (2010) Graphene and graphene oxide: synthesis, properties, and applications. *Adv. Mater.*, **22**, 3906–3924.

117. Lu, X.K., Yu, M.F., Huang, H., and Ruoff, R.S. (1999) Tailoring graphite with the goal of achieving single sheets. *Nanotechnology*, **10**, 269–272.

118. Li, X.S., Cai, W.W., An, J.H., Kim, S., Nah, J., Yang, D.X., Piner, R., Velamakanni, A., Jung, I., Tutuc, E., Banerjee, S.K., Colombo, L., and Ruoff, R.S. (2009) Large-area synthesis of high-quality and uniform graphene films on copper foils. *Science*, **324**, 1312–1314.

119. Kim, K.S., Zhao, Y., Jang, H., Lee, S.Y., Kim, J.M., Kim, K.S., Ahn, J.H., Kim, P., Choi, J.Y., and Hong, B.H. (2009) Large-scale pattern growth of graphene films for stretchable transparent electrodes. *Nature*, **457**, 706–710.

120. Berger, C., Song, Z.M., Li, X.B., Wu, X.S., Brown, N., Naud, C., Mayou, D., Li, T.B., Hass, J., Marchenkov, A.N., Conrad, E.H., First, P.N., and de Heer, W.A. (2006) Electronic confinement and coherence in patterned epitaxial graphene. *Science*, **312**, 1191–1196.

121. Park, S. and Ruoff, R.S. (2009) Chemical methods for the production of graphenes. *Nat. Nanotechnol.*, **4**, 217–224.

122. Ren, W.C. and Cheng, H.M. (2014) The global growth of graphene. *Nat. Nanotechnol.*, **9**, 726–730.

123. Ferrari, A.C. and Basko, D.M. (2013) Raman spectroscopy as a versatile tool for studying the properties of graphene. *Nat. Nanotechnol.*, **8**, 235–246.
124. Georgakilas, V., Otyepka, M., Bourlinos, A.B., Chandra, V., Kim, N., Kemp, K.C., Hobza, P., Zboril, R., and Kim, K.S. (2012) Functionalization of graphene: covalent and non-covalent approaches, derivatives and applications. *Chem. Rev.*, **112**, 6156–6214.
125. Cai, W.W., Piner, R.D., Stadermann, F.J., Park, S., Shaibat, M.A., Ishii, Y., Yang, D.X., Velamakanni, A., An, S.J., Stoller, M., An, J.H., Chen, D.M., and Ruoff, R.S. (2008) Synthesis and solid-state NMR structural characterization of ^{13}C-labeled graphite oxide. *Science*, **321**, 1815–1817.
126. Gao, W., Alemany, L.B., Ci, L.J., and Ajayan, P.M. (2009) New insights into the structure and reduction of graphite oxide. *Nat. Chem.*, **1**, 403–408.
127. Bekyarova, E., Itkis, M.E., Ramesh, P., Berger, C., Sprinkle, M., de Heer, W.A., and Haddon, R.C. (2009) Chemical modification of epitaxial graphene: spontaneous grafting of aryl groups. *J. Am. Chem. Soc.*, **131**, 1336–1337.
128. Liu, H.T., Ryu, S.M., Chen, Z.Y., Steigerwald, M.L., Nuckolls, C., and Brus, L.E. (2009) Photochemical reactivity of graphene. *J. Am. Chem. Soc.*, **131**, 17099–17101.
129. Sofo, J.O., Chaudhari, A.S., and Barber, G.D. (2007) Graphane: a two-dimensional hydrocarbon. *Phys. Rev. B*, **75**, 153401.
130. Boukhvalov, D.W., Katsnelson, M.I., and Lichtenstein, A.I. (2008) Hydrogen on graphene: electronic structure, total energy, structural distortions and magnetism from first-principles calculations. *Phys. Rev. B*, **77**, 035427.
131. Sahin, H., Topsakal, M., and Ciraci, S. (2011) Structures of fluorinated graphene and their signatures. *Phys. Rev. B*, **83**, 115432.
132. Elias, D.C., Nair, R.R., Mohiuddin, T.M.G., Morozov, S.V., Blake, P., Halsall, M.P., Ferrari, A.C., Boukhvalov, D.W., Katsnelson, M.I., Geim, A.K., and Novoselov, K.S. (2009) Control of graphene's properties by reversible hydrogenation: evidence for graphane. *Science*, **323**, 610–613.
133. Nair, R.R., Ren, W.C., Jalil, R., Riaz, I., Kravets, V.G., Britnell, L., Blake, P., Schedin, F., Mayorov, A.S., Yuan, S.J., Katsnelson, M.I., Cheng, H.M., Strupinski, W., Bulusheva, L.G., Okotrub, A.V., Grigorieva, I.V., Grigorenko, A.N., Novoselov, K.S., and Geim, A.K. (2010) Fluorographene: a two-dimensional counterpart of teflon. *Small*, **6**, 2877–2884.
134. Kashtiban, R.J., Dyson, M.A., Nair, R.R., Zan, R., Wong, S.L., Ramasse, Q., Geim, A.K., Bangert, U., and Sloan, J. (2014) Atomically resolved imaging of highly ordered alternating fluorinated graphene. *Nat. Commun.*, **5**, 4902.
135. Zhang, L.M., Lu, Z.X., Zhao, Q.H., Huang, J., Shen, H., and Zhang, Z.J. (2011) Enhanced chemotherapy efficacy by sequential delivery of siRNA and anticancer drugs using PEI-grafted graphene oxide. *Small*, **7**, 460–464.
136. Yang, K., Feng, L.Z., Shi, X.Z., and Liu, Z. (2013) Nano-graphene in biomedicine: theranostic applications. *Chem. Soc. Rev.*, **42**, 530–547.
137. Wang, Y., Li, Z.H., Wang, J., Li, J.H., and Lin, Y.H. (2011) Graphene and graphene oxide: biofunctionalization and applications in biotechnology. *Trends Biotechnol.*, **29**, 205–212.
138. Liu, Z., Robinson, J.T., Sun, X.M., and Dai, H.J. (2008) PEGylated nanographene oxide for delivery of water-insoluble cancer drugs. *J. Am. Chem. Soc.*, **130**, 10876–10877.
139. Zhang, S.A., Yang, K., Feng, L.Z., and Liu, Z. (2011) In vitro and in vivo behaviors of dextran functionalized graphene. *Carbon*, **49**, 4040–4049.
140. Gollavelli, G. and Ling, Y.C. (2012) Multi-functional graphene as an in vitro and in vivo imaging probe. *Biomaterials*, **33**, 2532–2545.